Feasibility Study of Prestress Force Prediction for Concrete Beams Using Second-Order Deflections

Marco Bonopera[a,d*], Kuo-Chun Chang[b], Chun-Chung Chen[a], Yu-Chi Sung[a,c] and Nerio Tullini[d]

[a]*Bridge Division, National Center for Research on Earthquake Engineering*

No. 200, Sec. 3, Xinhai Road, Taipei, 10668, Taiwan

[b]*Department of Civil Engineering, National Taiwan University*

No. 1, Sec. 4, Roosevelt Road, Taipei, 10617, Taiwan

[c]*Department of Civil Engineering, National Taipei University of Technology*

No. 1, Sec. 3, Zhongxiao E. Road, Taipei, 10608, Taiwan

[d]*Department of Engineering, University of Ferrara*

No. 1, Via Saragat, Ferrara, 44122, Italy

*Corresponding author - *E-mails:* bonopera@ncree.narl.org.tw - marco.bonopera@unife.it

Authors - *E-mails:* ciekuo@ntu.edu.tw - ccchen@ncree.narl.org.tw - sungyc@ntut.edu.tw - nerio.tullini@unife.it

The safety and sustainability of prestressed concrete bridges can be improved with accurate prestress loss prediction. Considerable loss of the prestress force may imply damages hidden in the bridge. In this study, a prestress force identification method was implemented for concrete beams. Based on the Euler–Bernoulli beam theory, the procedure estimates the prestress force by using one or a set of static displacements measured along the member axis. The implementation of this procedure requires information regarding the flexural rigidity of the beam. The deflected shape of a post–tensioned concrete beam, subjected to an additional vertical load, was measured in a short term in several laboratory experiments. The accuracy of the deflection measurements provided favorable prestress force estimates. In particular, the "compression–softening" theory was validated for uncracked post–tensioned concrete beams.

Keywords: Concrete beam; force prediction; inverse problem; prestress loss; second-order theory; static test.

1. Introduction

Nondestructive testing (NDT) methods are generally used for determining the condition of concrete elements for preventive maintenance, repair, or replacement of a bridge. An accurate evaluation of the *in situ* prestress axial force is required to monitor prestress losses in concrete bridge beams. Therefore, the operating state of bridge decks must be controlled using NDT methods to support safety assessments during the service life of the decks. Substantial losses of prestress forces may indicate damage phenomena; however, prestress forces (and losses) can be directly, simply, and accurately estimated if the internal tendons of concrete beams are instrumented using a load cell during construction.[1,2] Although instrumentation of external tendons is easy during their service life, NDT methods are generally required for this process.

Axial force identification in externally loaded beams has been studied using nondestructive static and dynamic methods.[3-10] In particular, for vibration-based estimations of axial loads, an accurate flexural mode shape must be selected for the identification process.[4,8] Such methods are particularly sensitive to experimental and model errors. Moreover, selecting the optimal frequency *a priori* to estimate the axial load is challenging, and different natural frequencies yield varying degrees of accuracy in axial force estimations.

The effect of the prestress force on the dynamic behavior of prestressed members has been discussed, including in a literature review by Noble *et al.*[11,12] Several studies, including those by Miyamoto *et al.*,[13] Law and Lu,[14] and Lu and Law,[15] have assumed that the prestress force in the strand is equivalent to an external axial load assigned to each beam end. Consequently, the natural vibration frequency of the post-tensioned structure tends to decrease with an increase in the prestress force; this is termed the compression-softening effect. This effect occurs in externally axially loaded Euler–Bernoulli beams prone to buckling failure.[3,9,10] The opposite phenomenon concerning axial tension is termed the tension-stiffening effect because it occurs in tension members within the elastic range.[3,7] By contrast, Hamed and Frostig[16] suggested that the natural frequency of a prestressed beam is unaffected by the prestress force. The researchers claimed that the original line of action of the prestress force is modified during vibration of the member, thereby preserving the eccentricity of the force with respect to the beam axis. Accordingly, a prestress force does not cause Euler buckling; therefore, the external axial compressive force retains its original line of action, varying only the eccentricity of the force with respect to the beam axis during vibrational displacement.

To identify the existing prestress force in concrete beams, Abraham *et al.*,[17] Kim *et al.*,[18,19] Bu and Wang,[20] Xu and Sun,[21] and Shi *et al.*[22] have presented vibration methods based on the modal frequencies and dynamic responses of structures. Law *et al.*[23] and Li *et al.*[24] have performed numerical simulations using the dynamic responses of structures to moving vehicular loads. Capozucca[25] investigated prestress loss in members subjected to damage due to reinforcement corrosion, whereas Limongelli *et al.*[26] studied the detection of early warning signs of deterioration in a concrete beam due to prestress loss. A beam's natural frequencies are used as parameters in NDT methods; specifically, because the prestress force does not substantially affect these frequencies, loss estimation is not particularly accurate. Therefore, natural frequency cannot be considered a suitable indicator for detecting prestress loss, as demonstrated previously.[27]

In this study, the static NDT method proposed by Bonopera *et al.*[10] was employed for prestress load identification in prismatic concrete beams. The reference model comprised a simply supported Euler–Bernoulli beam prestressed using a straight unbonded tendon, where the prestress load was assumed to be an external axial load applied eccentrically to the beam ends, based on the compression-softening theory. In a related study, Reis *et al.*[28] studied an approach based on the natural period of vibration to consider second-order effects in concrete frames. Furthermore, some static NDT methods, based on the second-order theory, have been developed to detect the axial load in steel members.[5,6,9] In the present feasibility study, the vertical displacement obtained from a three-point bending test conducted on the aforementioned post-tensioned beam was approximated by multiplying the first-order deflection by the magnification factor of the second-order effects,[29,30] in accordance with predictions based on the compression-softening theory. First, deflected-shape measurements along the beam length, obtained from 27 three-point bending tests, were examined to assess the accuracy of the beam mechanical model assumptions. Small displacements were imposed to prevent crack formation in the concrete beam. Subsequently, the NDT method proposed by Bonopera *et al.*[10] based on the aforementioned magnification factor approach was employed to identify the prestress force. In particular, the prestress force was estimated using one or a set of the deflected-shape measurements. This method requires information regarding the flexural rigidity of the beam. The NDT method uses only static parameters; thus, in contrast to dynamic procedures, this method does not require selecting experimental data for use in algorithms. The detected prestress force verified the feasibility of the procedure in the presence of moderate measurement errors. The NDT method used in this study can be applied to concrete beams subjected to prestress force to satisfy the decompression serviceability limit state. Finally, the constraint stiffness of the beam ends must be evaluated for prestressed concrete members with unknown boundary conditions.

2. NDT method proposed by Bonopera *et al.*[10]

2.1. Analytical model

Figure 1 illustrates the formulation of the NDT method proposed by Bonopera *et al.*,[10] which focuses on a simply supported prestressed member of length L. The end constraints of a prismatic concrete beam are often known, as are those of the prestressed beam of a bridge deck. The length of these simply supported elements can be measured *in situ* or obtained from corresponding project drawings. The beam is first subjected to an eccentric prestress force N (with eccentricity e) with respect to the centroid of the cross section (Fig. 1(a)) and subsequently to a vertical load F at the midspan (Fig. 1(b)). The prestress force N is assumed to be externally applied. The elastic modulus E of concrete and the cross-sectional second moment of area I are assumed to be known parameters.

The initial deflection curve $v^{(0)}$ (Fig. 1(a)) after the application of the eccentric prestress force N can be expressed as follows:[29,30]

$$v^{(0)}(x) = e\left[1-\cos\sqrt{n}\left(\frac{1}{2}-\frac{x}{L}\right)\Big/\cos(\sqrt{n}/2)\right] \quad (1)$$

where $n = NL^2/EI$ is the nondimensional axial force. Subsequently, a point load F is applied to the initial deflection curve $v^{(0)}$. The corresponding bending moments in the left and right portions of the beam (Fig. 1(b)) are respectively expressed as follows:

$$M = F\,x/2 + N\,(v^{(1)} - e) \text{ for } 0 \le x \le L/2, \tag{2a}$$

$$M = F\,(L - x)/2 + N\,(v^{(1)} - e) \text{ for } L/2 \le x \le L. \tag{2b}$$

Incorporating Eqs. (2a) and (2b) into the expression for the beam axis curvature $M = -EI\, \mathrm{d}^2v^{(1)}/\mathrm{d}x^2$ yields the solution $v^{(1)} = v^{(0)} + v_{\text{tot}}^{(a)}$, where $v_{\text{tot}}^{(a)}$ is the deflection curve of the beam under the concentric axial load N and vertical load F (Fig. 1(c)),[29,30,6] which can be expressed as follows:

$$v_{\text{tot}}^{(a)}(x) = \frac{\psi}{2\sqrt{n^3}}\left[\frac{1}{\cos\sqrt{n}/2}\sin\left(\sqrt{n}\,\frac{x}{L}\right) - \sqrt{n}\,\frac{x}{L}\right] \text{ for } 0 \le x \le L/2, \tag{3a}$$

$$v_{\text{tot}}^{(a)}(x) = \frac{\psi}{2\sqrt{n^3}}\left\{\frac{1}{\cos\sqrt{n}/2}\sin\left[\sqrt{n}\,\left(1-\frac{x}{L}\right)\right] - \sqrt{n}\,\left(1-\frac{x}{L}\right)\right\} \text{ for } L/2 \le x \le L, \tag{3b}$$

where $\psi = FL^3/EI$ is the load parameter with a length dimension. Deflections measured in the experiments performed in this study were compared with the analytical solution, $v_{\text{tot}}^{(a)} = v^{(1)} - v^{(0)}$, generated using Eqs. (3a) and (3b). As n approaches 0, the limit of Eqs. (3a) and (3b) yields the first-order displacement $v_{\mathrm{I}}^{(a)}$ (neglecting the effect of the external prestress force), which can be expressed as follows:

$$v_{\mathrm{I}}^{(a)}(x) = \frac{\psi}{12}\frac{x}{L}\left[\frac{3}{4} - \left(\frac{x}{L}\right)^2\right] \text{ for } 0 \le x \le L/2, \tag{4a}$$

$$v_{\mathrm{I}}^{(a)}(x) = \frac{\psi}{12}\left(1-\frac{x}{L}\right)\left[\frac{2x}{L} - \left(\frac{x}{L}\right)^2 - \frac{1}{4}\right] \text{ for } L/2 \le x \le L. \tag{4b}$$

2.2. Identifying the prestress force through one displacement measurement

The total vertical displacement in Eqs. (3a) and (3b) is well approximated by multiplying the first-order deflections obtained in Eqs. (4a) and (4b) by the magnification factor of the second-order effects, $1/(1 - N/N_{\mathrm{crE}})$,[29,30] which can be expressed as follows:

$$v_{\mathrm{tot}}^{(x)}(x) = \frac{v_{\mathrm{I}}^{(a)}(x)}{1 - N/N_{\mathrm{crE}}}, \tag{5}$$

where $N_{\mathrm{crE}} = \pi^2 EI/L^2$ is the first Euler buckling load for the simply supported beam. Thus, the magnification factor of the second-order effects coincides with the ratio $v_{\mathrm{I}}^{(a)}(x)/v_{\mathrm{tot}}^{(x)}(x)$.

A three-point bending test with an assigned prestress force N can be conducted to measure the vertical displacement $v_{\mathrm{tot}}^{(x)}(x)$. Consequently, the ratio $v_{\mathrm{I}}^{(a)}(x)/v_{\mathrm{tot}}^{(x)}(x)$ and the definition of the magnification factor can be used to calculate the prestress (or compressive) force N_a in Euler–Bernoulli beam columns using the following equation:[9]

$$N_a = N_{\mathrm{crE}} \left(1 - \frac{v_{\mathrm{I}}^{(a)}(x)}{v_{\mathrm{tot}}^{(x)}(x)} \right). \tag{6}$$

By incorporating the nondimensional axial force $n_a = N_a L^2/EI$ into Eq. (6), the following expression is obtained:

$$n_a = \pi^2 \left(1 - \frac{v_{\mathrm{I}}^{(a)}(x)}{v_{\mathrm{tot}}^{(x)}(x)} \right). \tag{7}$$

When the point load F is applied at the midspan of the beam, Eq. (4a) yields the first-order displacement at a quarter of the span, $v_{\mathrm{I}}^{(a)}(L/4) = 11\psi/768$, and the first-order midspan displacement, $v_{\mathrm{I}}^{(a)}(L/2) = \psi/48$. Thus, Eq. (7) can be rewritten as follows:

$$n_a = \pi^2 \left(1 - \frac{11\psi}{768\, v_{\mathrm{tot}}^{(x)}(L/4)} \right) \quad \text{or} \quad n_a = \pi^2 \left(1 - \frac{\psi}{48\, v_{\mathrm{tot}}^{(x)}(L/2)} \right). \tag{8a, b}$$

In summary, load identification must be conducted through the following stages:

(1) Measure the displacement at the quarter cross section $v_{\text{tot}}^{(x)}(L/4)$ following the application of load F or measure the corresponding displacement at the midspan $v_{\text{tot}}^{(x)}(L/2)$,

(2) Solve Eq. (8a) or (8b) for the unknown constant n_a using the displacement $v_{\text{tot}}^{(x)}(L/4)$ or $v_{\text{tot}}^{(x)}(L/2)$ and the expression for ψ, and

(3) Determine the analytical value of the prestress force, $N_a = n_a\, EI/L^2$.

Equations (8a) and (8b) do not require the initial prestress force value, and thus the need to install equipment in the internal tendon is obviated.

2.3. Identifying the prestress force through a set of displacement measurements

If a set of displacements $v_{\text{tot}}^{(x)}(x_i)$ for i = 1, …, m is measured along the beam length, the prestress force value N_a that minimizes the standard deviation between the experimental displacement $v_{\text{tot}}^{(x)}(x_i)$ and first-order displacement $v_{\text{I}}^{(a)}(x_i)$ can be identified; in other words, it is possible to obtain N_a such that

$$\min_{N_a} \sum_{i=1}^{m} \left[v_{\text{tot}}^{(x)}(x_i) - \frac{v_{\text{I}}^{(a)}(x_i)}{1 - N_a/N_{\text{crE}}} \right]^2 . \tag{9}$$

This problem can be solved by setting the derivative of Eq. (9) with respect to N_a as 0 to obtain the following expression:

$$N_a = N_{\text{crE}} \frac{\sum_{i=1}^{m} v_{\text{I}}^{(a)}(x_i)\, v_{\text{tot}}^{(x)}(x_i) \left[1 - \dfrac{v_{\text{I}}^{(a)}(x_i)}{v_{\text{tot}}^{(x)}(x_i)} \right]}{\sum_{i=1}^{m} v_{\text{I}}^{(a)}(x_i)\, v_{\text{tot}}^{(x)}(x_i)} . \tag{10}$$

In this additional test configuration, the load identification process must be conducted through the following stages:

(1) Measure a set of displacements $v_{\mathrm{tot}}^{(x)}(x_i)$ along the beam length after applying load F,

(2) Determine the first Euler buckling load $N_{\mathrm{crE}} = \pi^2 EI/L^2$, and

(3) Solve Eq. (10) to obtain the prestress force N_a by computing the set of first-order displacements $v_{\mathrm{I}}^{(a)}(x_i)$ using Eqs. (4a) and (4b).

The additional load F can be located at various cross sections; therefore, the first-order displacement $v_{\mathrm{I}}^{(a)}(x_i)$ and experimental displacements $v_{\mathrm{tot}}^{(x)}(x_i)$ must be evaluated in relation to any cross section along the beam length. Various boundary conditions can be applied by assuming the appropriate Euler buckling load N_{crE} in Eq. (6) or (10) after experimentally determining the beam end stiffness. Concrete bridge beams under real conditions, where end stiffness cannot be easily evaluated, will be investigated in future studies.

3. Description of post-tensioned concrete beam specimen and test layout

A post-tensioned concrete beam with a 250-mm × 400-mm rectangular cross section was used. The beam was reinforced longitudinally with two top bars and two bottom bars and transversely with 44 stirrups each at a distance of 150 mm. The strand had a small eccentricity of 50 mm with respect to the cross section centroid and comprised seven tendons, thereby composing a seven-wire strand (diameter = 15.2 mm) inserted into seven distinct plastic ducts and embedded in the concrete cross section. The plastic ducts were not injected. The ultimate yield strength of the tendons was 1860 MPa. A support was positioned at each beam end to create pinned-end restraints (Fig. 2(c) and (d)), resulting in a clear span L of 6.62 m (Fig. 3). For the rectangular concrete cross section I_{exact}, the cross-sectional second moment of the area and slenderness ratio were 1.3333×10^9 mm^4 and 57, respectively. When the beam was positioned on the supports, all geometric dimensions were verified using measurement systems with 0.01-mm tolerance (laser rangefinder and caliper). The elastic modulus of the concrete was experimentally evaluated through compression tests after 28 days of curing and on each day of NDT method simulation in the laboratory.

The post-tensioned concrete beam was inserted into a test frame using a test rig (Fig. 4(a)). At one beam end, a hydraulic oil jack with a 4000-kN force capacity was used to apply the prestress force by pulling the strand outward. A 1000-kN load cell with 2-mV/V accuracy was positioned at the other end to measure the applied prestress force (Fig. 2(a)). Prestress forces of approximately 618, 722, and 820 kN were applied; for each prestress force, an additional vertical load F was applied using a hydraulic actuator at the midspan of the beam with an initial value of approximately 20.0 kN, which was gradually increased to approximately 22.5 and then approximately 25.0 kN (Fig. 2(b)). The final test condition was repeated three times, yielding a total of 27 tests. The concrete beam did not develop any cracks during the tests.

On the basis of the test layout, nine linear variable differential transformer (LVDT) sensors were positioned along the beam length corresponding to the cross sections at i = 0, …, 8, as illustrated in Figs. 4(b) and 5. Steel plates were used to locate each LVDT sensor corresponding to the beam axis (Fig. 4(b)). A reference LVDT sensor, labeled "R.P." in Fig. 5, was positioned at both beam ends, at i = 0 and 8 (Fig. 2(c) and (d)). These two LVDT sensors served as references for the displacement measurement system to form a reference line for measurements between the end supports. Moreover, all LVDTs were connected to a data logger located on a desk close to the test rig.

All test measurements were recorded once per second for approximately 200 s using a data acquisition unit. The average measurements of the prestress forces $N_{x,aver}$ and vertical loads F_{aver} were considered for each test combination.

4. Experimental and numerical simulations of the NDT method proposed by Bonopera *et al.*[10]

4.1. Evaluation of the time-dependent elastic modulus of concrete

Regarding the post-tensioned beam, a set of 150 mm × 300 mm concrete cylinders were cast to measure the time-dependent elastic modulus of the used concrete through compression tests. The beam and all cylindrical specimens were maintained under the same curing environmental conditions specifically, outdoor laboratory spaces. The elastic modulus E of each single cylinder was estimated using Eq. (11) in accordance with ASTM Standard C 469/C 469M–14. Equation (11) is expressed as follows:[31]

$$E = \frac{\sigma_2 - \sigma_1}{\varepsilon_2 - 0.00005}, \tag{11}$$

where σ_1 and σ_2 are the stress levels corresponding to the longitudinal strain of 0.00005 and 40% of the ultimate longitudinal compressive stress, respectively, and ε_2 is the longitudinal strain produced by σ_2. These three values were determined based on graphs depicting longitudinal compressive stress versus longitudinal strain for the single cylinders. One compressometer equipped with two LVDT sensors was used as the strain measurement system. The universal testing machine was set at a loading rate of approximately 1 mm/min.

The measured elastic modulus E of the concrete at 28 days and that during the execution of the NDT method in the laboratory are listed in Table 1. The average elastic modulus value E_{aver} was calculated on specific days as desired by testing two cylinders. By contrast, three specimens were tested during 28 days of curing. The average elastic modulus E_{aver} exhibited progressive increments of 14.1%, 23.1%, and 26.9% with respect to the value obtained after 28 days. The mean characteristic strength f_{ck} was 66.27 MPa for all compression tests detailed in Table 1.

In the NDT method,[10] as described in the previous section, the elastic modulus E of the simply supported beam is a known parameter. However, concrete members in civil structures generally have scattered values along their axes. A numerical three-point bending test was performed to determine the effect of the elastic modulus on the prestress force estimation. Reference was made to Eq. (8b) and the E_{ref} value of 37,093 MPa, which was calculated from the average elastic modulus E_{aver} obtained through compression tests conducted after 426, 427, and 433 days of curing (Table 1). Table 2 presents the load parameter ψ and second-order midspan deflections v_4 of the post-tensioned beam evaluated for four prestress forces N_x using Eqs. (3a) and (3b). The maximum prestress force that did not induce crack formation was 1050 kN. Figure 6 shows that the estimated prestress force N_a was sensitive to small variations in the elastic modulus

E_{ref}. The difference in N_a was greater than the corresponding variation imposed on E_{ref}. For N_x = 1050 kN, the estimated N_a increased by 9.7% and decreased by 11.5% when E_{ref} increased and decreased by 1%, respectively. These results demonstrate that conducting compression tests on drilled concrete cores from an existing beam in accordance with ASTM Standards C 469/C 469M–14[31] and C 42/C 42M–13[31] is the only procedure ensuring high accuracy when estimating the elastic modulus through the NDT method.[10] An objective of further research is to define the drilling position of a set of concrete cores to determine the most reliable elastic modulus along the axis of concrete bridge beams.

4.2. Deflected-shape measurements

The displacements v_i for i = 1, …, 7 in the post-tensioned concrete beam served as parameters for the algorithms of the NDT method[10] (Eqs. (8) and (10)). Specifically, the displacements v_i located in accordance with the test layout shown in Fig. 5 were recorded after the additional load F had been applied. Thus, the initial deflection reference shape was assumed to be the one with the assigned prestress force N_0 (Fig. 1(a)); this condition represented the operation stage for an existing bridge deck. Each prestress force N_x prevented the concrete beam from developing cracks under the vertical load F. During testing, the average prestress force $N_{x,aver}$ of 820 kN was 78.1% of the maximum prestress force N_x; this satisfied the decompression serviceability limit state of 1050 kN.

Table 3 compares the measured displacements v_i with the corresponding analytical values $v_{\mathrm{tot}}^{(a)}(x)$ obtained using Eqs. (3a) and (3b). Figure 7 displays the deflection shape for three prestress forces $N_{x,aver}$ for F_{aver} = 25.1 kN. The cross-sectional second moment of the area I_{exact} and elastic modulus E_{aver} for each day of execution of the NDT method[10] were assumed for computation (Table 1). A decrease in the displacements v_i with an increase in the prestress force N_x was caused by an increment in the flexural rigidity due to an increase in the elastic modulus E_{aver} (Table 1). Table 3 illustrates several measurements, namely the initial prestress forces N_0, prestress forces N_x when the loads F were applied, and vertical loads F. In several dynamic tests, the natural frequencies (and flexural rigidities) increased with the magnitude of the prestress force,[32,33,19] thereby contradicting the compression-softening theory. Nonetheless, the displacements and natural frequencies were sensitive to the variation in the elastic modulus of concrete over time.

In all 27 test combinations, favorable repeatability was achieved, with a relative error lower than 5.0% for all displacement measurements. The measured displacement v_5 for the combination of N_x = 620 kN and F = 20.2 and 22.6 kN was not considered because of loss of verticality in the LVDT sensor (Table 3). The measured displacement v_1 exhibited a systematic error with a mean value of 0.28 mm because of an LVDT sensor malfunction. The symmetric displacement v_7 had an absolute mean error of 0.02 mm.

Excluding the measured displacement v_1, the absolute mean error between the analytical and experimental displacements was 0.03 mm, corresponding to a relative error of −0.5%, which validated the effectiveness of using an LVDT sensor measurement system. Figure 8 displays values of the factor $1-v_{\text{tot}}^{(a)}/v_i$ for the cross sections at i = 2, 4, and 6. A maximum error of −8.5% was recorded for nine tests when $N_{x,aver}$ = 615 kN was applied. Displacements $v_{\text{tot}}^{(a)}(x)$ were similarly obtained using Eqs. (3a) and (3b). The errors were considerably lower at higher prestress forces. Thus, the compression-softening theory remains valid even when small flexural displacements are involved and crack formation is precluded. The first Euler buckling load of the post-tensioned beam, namely $N_{\text{crE}} = \pi^2 E_{ref} I_{exact}/L^2$, was 11,138 kN. Thus, the maximum prestress force $N_{x,aver}$ of 820 kN was only 7.4% of N_{crE}. Consequently, the first-order displacements were magnified by a factor of 1/(1 − 0.074) = 1.08. The prestress force N_x of 1050 kN corresponding to the maximum decompression serviceability limit state induced a magnification factor of 1.10. These conditions require accurate displacement measurements because the second-order effects are generally neglected when magnification factors lower than 1.10 are induced.

4.3. Prestress force identification

The values of the average prestress nondimensional forces $n_{a,aver}$ are listed in Table 4 and were obtained using the experimental values of $\psi = FL^3/E_{aver} I_{exact}$ and v_2 (Test 1) in Eq. (8a), as well as the same parameter ψ and v_4 (Test 2) in Eq. (8b) for each thrice-repeated test combination. The daily elastic modulus E_{aver} (Table 1) was used as a parameter in the load identification process. Table 5 illustrates the prestress forces $N_{a,aver}$ obtained using Eq. (10), particularly the mean values calculated for each test combination. The deflection sets of v_3-v_4-v_5 (Test 3), v_2-v_3-v_4-v_5-v_6 (Test 4), and v_1-v_2-v_3-v_4-v_5-v_6-v_7 (Test 5) recorded for each combination were computed as parameters for displacements $v_{\mathrm{tot}}^{(x)}(x_i)$. The first Euler buckling load, $N_{\mathrm{crE}} = \pi^2 E_{aver} I_{exact}/L^2$, was calculated for each day during the simulation of the NDT method. The corresponding first-order displacements $v_{\mathrm{I}}^{(a)}(x_i)$ were instead calculated using Eqs. (4a) and (4b). Moreover, the daily elastic modulus E_{aver} (Table 1) was used in the load estimation process.

Tables 4 and 5 illustrate the percentage errors $\Delta_{aver} = (N_{a,aver} - N_{x,aver})/N_{x,aver}$. Of all 27 test combinations, Test 5, which had a set of seven deflections (Fig. 5), yielded the most accurate load estimates $N_{a,aver}$. In general, poor load estimates $N_{a,aver}$ were obtained when $N_{x,aver}$ = 618 kN was applied. By contrast, the test combinations with prestress forces that induced second-order effects greater than 6.5% provided excellent load estimates $N_{a,aver}$ for Tests 2 and 5. Notably, all prestress force estimation errors were lower than 5.5%.

Sensitivity analyses were performed for load estimations based on Eqs. (8a) and (8b), corresponding to Tests 1 and 2, respectively. The values v_2 and v_4 obtained using Eqs. (3a) and (3b) and parameter ψ were modified to reproduce potential experimental errors. The values v_2, v_4, and ψ were alternatively multiplied by 0.99 and 1.01 to generate 14 combinations of simulated values for nine distinct assumed prestress forces N_x. The average value of the applied vertical loads in the process was assumed to be F_{aver} = 22.7 kN. Figure 9(a) and (b) illustrate a comparison between the worst estimated N_a and assumed values N_x conducted using displacements v_2 and v_4, both of which yielded a constant error of approximately ±107 kN. Furthermore, a comparison between the measured $N_{x,aver}$ and estimated values $N_{a,aver}$ based on the experiments (Table 4) is also depicted in Fig. 9(a) and (b). Favorable correspondence between the analytical N_x and experimental load estimates N_a was observed when the midspan deflection v_4 was considered.

5. Conclusions

This paper describes a feasibility study of applying the NDT method proposed by Bonopera *et al.*[10] to prestressed concrete beams. The method can detect the prestress force in a concrete member with a straight unbonded tendon based on static deflections. Displacements of a post-tensioned concrete beam subjected to a three-point bending test were measured in the short term through several laboratory experiments. The LVDT displacement measuring system achieved high accuracy, yielding reliable load estimates. The compression-softening theory was valid for post-tensioned concrete beams preserved by crack formation and when the magnification factor of the second-order effects was lower than 1.10. Subsequently, the experimental results demonstrated that midspan displacement should be employed in the load estimation process. If numerous displacements are considered and the induced second-order effects are greater than 6.5%, the accuracy of load estimation is substantially improved. Accurate information regarding the flexural rigidity of the prestressed concrete beam under investigation is necessary; in particular, the elastic modulus must be evaluated through compression tests on the drilled concrete cores. No direct measure of the tendon tensile force in the internal tendon is required.[1,2] Furthermore, no distinction between short- and long-term losses is required because the NDT method[10] can instantaneously identify the existing prestress force. Future studies could conduct experimental investigations involving three-point bending tests with vehicle loading on concrete bridge decks[34,35] and utilize the high potential of fiber Bragg grating differential settlement measurement sensors.[36-39]

Acknowledgments

M.B. acknowledges the financial support of the “Summer Program in Taiwan Grant” in 2015, provided by the Ministry of Science and Technology of Taiwan for European Ph.D. candidates. N.T. acknowledges the financial support of the “Research Program FAR 2017” provided by the University of Ferrara. The experiments were executed at the National Center for Research on Earthquake Engineering (NCREE) and supported by funding from the National Applied Research

Laboratories Project of Taiwan (NCREE–06104A1700). Finally, special gratitude is extended to the technicians of NCREE and students of National Taiwan University, who provided considerable assistance to the authors.

References

1. M. Saiidi, J. Shields, D. O'Connor and E. Hutchens, Variation of prestress forces in a prestressed concrete bridge during the first 30 months, *PCI J.*, **41**(5) (1996) 66–72.
2. M. Saiidi, E. Hutchens and D. Gardella, Bridge Prestress Losses in Dry Climate, *J. Bridge Eng.*, **3**(3) (1998) 111–116.
3. N. Tullini and F. Laudiero, Dynamic identification of beam axial loads using one flexural mode shape, *J. Sound Vib.*, **318**(1–2) (2008) 131–147.
4. A. S. Bahra and P. D. Greening, Identifying multiple axial load patterns using measured vibration data, *J. Sound Vib.*, **330**(15) (2011) 3591–3605.
5. N. Tullini, G. Rebecchi and F. Laudiero, Bending tests to estimate the axial force in tie–rods, *Mech. Res. Commun.*, **44** (2012) 57–64.
6. N. Tullini, Bending tests to estimate the axial force in slender beams with unknown boundary conditions, *Mech. Res. Commun.*, **53** (2013) 15–23.
7. G. Rebecchi, N. Tullini and F. Laudiero, Estimate of the axial force in slender beams with unknown boundary conditions using one flexural mode shape, *J. Sound Vib.*, **332**(18) (2013) 4122–4135.
8. K. Maes, J. Peeters, E. Reynders, G. Lombaert and G. De Roeck, Identification of axial forces in beam members by local vibration measurements, *J. Sound Vib.*, **332**(21) (2013) 5417–5432.
9. M. Bonopera, K.C. Chang, C.C. Chen, T.K. Lin and N. Tullini, Compressive column load identification in steel space frames using second–order deflection–based methods, *Int. J. Struct. Stab. Dy.*, **18**(7) (2018) 1850092. DOI: 10.1142/S021945541850092X.

10. M. Bonopera, K.C. Chang, C.C. Chen, Z.K. Lee and N. Tullini, Axial load detection in compressed steel beams using FBG–DSM sensors, *Smart Struct. Syst.*, **21**(1) (2018). DOI: https://doi.org/10.12989/sss.2018.21.1.000.
11. D. Noble, M. Nogal, A. O'Connor and V. Pakrashi, Dynamic impact testing on post–tensioned steel rectangular hollow sections; An investigation into the "compression–softening" effect, *J. Sound Vib.*, **355** (2015) 246–263.
12. D. Noble, M. Nogal, A. O'Connor and V. Pakrashi, The effect of prestress force magnitude and eccentricity on the natural bending frequencies of uncracked prestressed concrete beams, *J. Sound Vib.*, **365** (2016) 22–44.
13. A. Miyamoto, K. Tei, H. Nakamura and J. W. Bull, Behavior of pre–stressed beam strengthened with external tendons, *J. Struct. Eng.*, **126**(9) (2000) 1033–1044.
14. S. S. Law and Z. R. Lu, Time domain responses of a pre–stressed beam and pre–stress identification, *J. Sound Vib.*, **288**(4–5) (2005) 1011–1025.
15. Z. R. Lu and S. S. Law, Identification of pre–stress force from measured structural responses, *Mech. Syst. Signal Process.*, **20**(8) (2006) 2186–2199.
16. E. Hamed and Y. Frostig, Natural frequencies of bonded and unbonded pre–stressed beams pre–stress force effects, *J. Sound Vib.*, **295**(1–2) (2006) 28–39.
17. M. A. Abraham, S. Park and N. Stubbs, Loss of prestress prediction based on nondestructive damage location algorithms, *Smart Struct. Mater.*, V. **2446** of Proceedings of SPIE (1995) 60–67.
18. J. T. Kim, Y. S. Ryu and C. B. Yun, Vibration based method to detect pre–stress loss in beam type bridges, *Smart Syst. Non-destr. Eval. Civil Infrastr.*, V. **5057** of Proceedings of SPIE (2003) 559–568.
19. J. T. Kim, C. B. Yun, Y. S. Ryu and H. M. Cho, Identification of prestress–loss in PSC beams using modal information, *Struct. Eng. Mech.*, **17**(3–4) (2004) 467–482.

20. J. Q. Bu and H. Y. Wang, Effective pre–stress identification for a simply supported PRC beam bridge by BP neural network method, *J. Vib. Shock*, **30**(12) (2011) 155–159.
21. J. Xu and Z. Sun, Pre–stress force identification for eccentrically pre–stressed concrete beam from beam vibration response, *Tech Science Press*, SL, **5**(2) (2011) 107–115.
22. L. Shi, H. He and W. Yan, Pre–stress force identification for externally pre–stressed concrete beam based on frequency equation and measured frequencies, *Math. Probl. Eng.* (2014) art. 840937.
23. S. S. Law, S. Q. Wu and Z. Y. Shi, Moving load and pre–stress identification using wavelet based method, *J. Appl. Mech.*, Transactions ASME, **75**(2) (2008) art. ID 021014.
24. H. Li, Z. Lv and J. Liu, Assessment of pre–stress force in bridges using structural dynamic responses under moving vehicles, *Math. Probl. Eng.* (2013) art. ID 435939.
25. R. Capozucca, Detection of damage due to corrosion in prestressed RC beams by static and dynamic tests, *Constr. Build. Mater.*, **22** (2008) 738–746.
26. M. P. Limongelli, D. Siegert, E. Merliot, J. Waeytens, F. Bourquin, R. Vidal, V. Le Corvec, I. Gueguen and L.M. Cottineau, Damage detection in a post tensioned concrete beam – Experimental investigation, *Eng. Struct.*, **128** (2016) 15–25.
27. O. R. Jaiswal, Effect of prestressing on the first flexural natural frequency of beams, *Struct. Eng. Mech.*, **28**(5) (2008) 515–524.
28. D. G. Reis, G. H. Siqueira, L. C. M. Vieira and R. D. Ziemian, Simplified approach based on the natural period of vibration for considering second–order effects on reinforced concrete frames, *Int. J. Struct. Stab. Dy.*, **17** (2017).
29. S. P. Timoshenko and J. M. Gere, *Theory of Elastic Stability* (McGraw–Hill, New York, 1961).
30. Z. P. Bazant and L. Cedolin, *Stability of Structures* (Oxford University Press, New York, 1991).

31. Annual Book of ASTM Standards, Section 4: Construction vol. 04.02. Concrete & aggregates, American Society for Testing & Materials (2016).

32. T. Hop, The effect of degree of prestressing and age of concrete beams on frequency and damping of their free vibration, *Mater. Struct.*, **24** (1991) 210–220.

33. M. Saiidi, B. Douglas and S. Feng, Prestress force effect on vibration frequency of concrete bridges, *J. Struct. Eng.*, **120**(7) (1994) 2233–2241.

34. Y. T. Chiu, T. K. Lin, H. H. Hung, Y. C. Sung and K. C. Chang, Integration of in–situ load experiments and numerical modeling in a long–term bridge monitoring system on a newly–constructed widened section of freeway in Taiwan, *Smart Struct. Syst.*, **13**(6) (2014) 1015–1039.

35. Y. C. Sung, T. K. Lin, Y. T. Chiu, K. C. Chang, K. L. Chen and C. C. Chang, A bridge safety monitoring system for prestressed composite box–girder bridges with corrugated steel webs based on in–situ loading experiments and a long–term monitoring database, *Eng. Struct.*, **126** (2016) 571–585.

36. K. C. Chang, Z. K. Lee and C. C. Chen, Structural assessment of a repaired cable bridge damaged in 1999 Chi–Chi earthquake, *Proceedings of the International Symposium on Engineering Lessons Learned from the 2011 Great East Japan Earthquake*, March 1–4, Tokyo, Japan (2012).

37. Z. K. Lee, Bridge safety monitoring integrated system with full optical fiber and the method for sensing thereof, *J.P. Patent No. 5542980* (2014).

38. Z. K. Lee, Bridge safety monitoring integrated system with full optical fiber and the method for sensing thereof, *U.S. Patent No. 9183739* (2015).

39. C. C. Lai, H. Y. Au, M. S. Y. Liu, S. L. Ho and H. Y. Tam, Development of level sensors based on fiber Bragg grating for railway track differential settlement measurement, *IEEE Sens. J.*, **16**(16) (2016) 6346–6350.

List of Tables:

List of Figures:

Fig. 1. Reference model of the prestressed concrete beam. (a) Deflection curve $v^{(0)}$ *after the application of the eccentric prestress force N, (b) deflection curve* $v^{(1)}$ *after the application of the vertical load F to deflection curve* $v^{(0)}$*, and (c) deflection curve* $v_{\mathrm{tot}}^{(a)}$ *after the application of the vertical load F. The dashed lines correspond to the initial deflection curves.*

Fig. 2. (a) Load cell at one beam end. (b) Hydraulic actuator at the midspan of the beam. (c) Reference LVDT sensor at hinge support. (d) Reference LVDT sensor at roller support.

Fig. 3. Scheme of the post–tensioned concrete beam specimen.

Fig. 4. (a) Test rig for the NDT method. (b) LVDT sensors along the beam length.

Fig. 5. Test layout with locations of the instrumented sections of the LVDT sensors (values in meters).

Fig. 6. Numerical three–point bending test. Estimated prestress forces N_a *versus elastic modulus E for the four assumed values* N_x *illustrated in Table 2.*

Fig. 7. Experimental three–point bending test. Deflection shape for three prestress forces $N_{x,aver}$ *for the* $F_{aver} = 25.1$ *kN.*

Fig. 8. Error $1 - v_{\mathrm{tot}}^{(a)}/v_i$ *versus test number for all test combinations and displacements* v_2*,* v_4*, and* v_6 *depicted in Fig. 5.*

Fig. 9. Prestress force estimates based on (a) Eq. (8a) - Test 1 and (b) Eq. (8b) - Test 2. Symbols + *refer to the comparison between estimated* N_a *and measured values* N_x *for all 27 test combinations. Symbols* × *refer to the estimated values* $N_{a,aver}$*. The dashed lines with symbol* × *refer to the sensitivity analyses.*

Table 1. Measured elastic modulus obtained through compression tests.

Day of concrete curing	Cylinder	E (MPa)	E_{aver} (MPa)	Variation (%)
28th	A	28734	30560	–
28th	B	32124		
28th	C	30823		
426th	1	34732	34870	+14.1
426th	2	35008		
427th	3	39602	37618	+23.1
427th	4	35634		
433rd	5	39407	38791	+26.9
433rd	6	38174		

Table 2. Analytical values of ψ and displacements v_4 evaluated using E_{ref} for four assumed values of the prestress force N_x.

N_x (kN)	F (kN)	ψ (mm)	v_4 (mm)
700	25.0	146.65	3.26
845	25.0	146.65	3.30
950	25.0	146.65	3.34
1050	25.0	146.65	3.37

Table 3. Comparison between analytical and measured displacements for each test execution day, corresponding to the layout depicted in Fig. 5.

Day of concrete curing	E_{aver} (MPa)	N_0 (kN)	N_x (kN)	F (kN)		v_1 (mm)	v_2 (mm)	v_3 (mm)	v_4 (mm)	v_5 (mm)	v_6 (mm)	v_7 (mm)
426th	34870	619	620	20.2	Analytical	1.03	1.92	2.55	2.79	2.55	1.92	1.03
					LVDT	1.45	1.95	2.62	2.84	-	1.93	1.02
426th	34870	619	620	22.6	Analytical	1.15	2.15	2.85	3.12	2.85	2.15	1.15
					LVDT	1.59	2.20	2.95	3.20	-	2.17	1.15
426th	34870	615	617	25.0	Analytical	1.27	2.38	3.16	3.45	3.16	2.38	1.27
					LVDT	1.42	2.32	3.12	3.43	3.03	2.27	1.22
427th	37618	723	724	20.1	Analytical	0.95	1.78	2.37	2.59	2.37	1.78	0.95
					LVDT	1.19	1.78	2.39	2.59	2.33	1.73	0.94
427th	37618	720	721	22.6	Analytical	1.07	2.00	2.66	2.91	2.66	2.00	1.07
					LVDT	1.31	2.00	2.67	2.92	2.60	1.94	1.05
427th	37618	720	721	25.1	Analytical	1.19	2.22	2.95	3.23	2.95	2.22	1.19
					LVDT	1.46	2.22	2.97	3.23	2.90	2.16	1.17
433rd	38791	820	820	20.2	Analytical	0.93	1.75	2.32	2.54	2.32	1.75	0.93
					LVDT	1.20	1.75	2.33	2.54	2.29	1.71	0.92
433rd	38791	820	820	22.9	Analytical	1.06	1.98	2.63	2.88	2.63	1.98	1.06
					LVDT	1.33	1.98	2.65	2.88	2.60	1.94	1.04
433rd	38791	820	820	25.1	Analytical	1.16	2.17	2.88	3.15	2.88	2.17	1.16
					LVDT	1.42	2.17	2.91	3.17	2.86	2.14	1.15

Table 4. Prestress force estimates based on Eqs. (8a) and (8b), and measured and estimated parameters for each test day obtained using displacements v_2 and v_4.

				Test 1 - v_2 deflection at a quarter			Test 2 - v_4 deflection at the midspan		
Day of concrete curing	E_{aver} (MPa)	$N_{x,aver}$ (kN)	F_{aver} (kN)	$n_{a,aver}$	$N_{a,aver}$ (kN)	Δ_{aver} (%)	$n_{a,aver}$	$N_{a,aver}$ (kN)	Δ_{aver} (%)
426th	34870	617	20.2	0.37	392	-36.5	0.38	399	-35.3
		618	22.7	0.46	490	-20.7	0.45	478	-22.7
		618	25.1	0.42	450	-27.2	0.49	516	-16.5
427th	37618	722	20.1	0.59	671	-7.1	0.62	715	-1.0
		722	22.7	0.62	709	-1.8	0.67	762	5.5
		722	25.1	0.57	649	-10.1	0.61	699	-3.2
433rd	38791	820	20.2	0.65	762	-7.1	0.70	822	0.2
		820	22.8	0.64	761	-7.2	0.67	797	-2.8
		820	25.1	0.63	740	-9.8	0.70	825	0.6

Table 5. Prestress force estimates based on Eq. (10), and measured and estimated parameters for each test day obtained using the sets v_3-v_4-v_5, v_2-v_3-v_4-v_5-v_6, and v_1-v_2-v_3-v_4-v_5-v_6-v_7.

					Test 3 v_3-v_4-v_5 three-deflections		Test 4 v_2-v_3-v_4-v_5-v_6 five-deflections		Test 5 v_1-v_2-v_3-v_4-v_5-v_6-v_7 seven-deflections	
Day of concrete curing	E_{aver} (MPa)	N_{crE} (kN)	$N_{x,aver}$ (kN)	F_{aver} (kN)	$N_{a,aver}$ (kN)	Δ_{aver} (%)	$N_{a,aver}$ (kN)	Δ_{aver} (%)	$N_{a,aver}$ (kN)	Δ_{aver} (%)
426th	34870	10471	617	20.2	400	-35.2	368	-40.4	453	-26.6
			618	22.7	480	-22.3	447	-27.7	524	-15.2
			618	25.1	485	-21.5	443	-28.3	512	-17.2
427th	37618	11296	722	20.1	644	-10.8	609	-15.7	706	-2.2
			722	22.7	696	-3.6	659	-8.7	745	3.2
			722	25.1	646	-10.5	611	-15.4	687	-4.8
433rd	38791	11648	820	20.2	743	-9.4	708	-13.7	811	-1.1
			820	22.8	749	-8.7	723	-11.8	811	-1.1
			820	25.1	767	-6.5	733	-10.6	809	-1.3

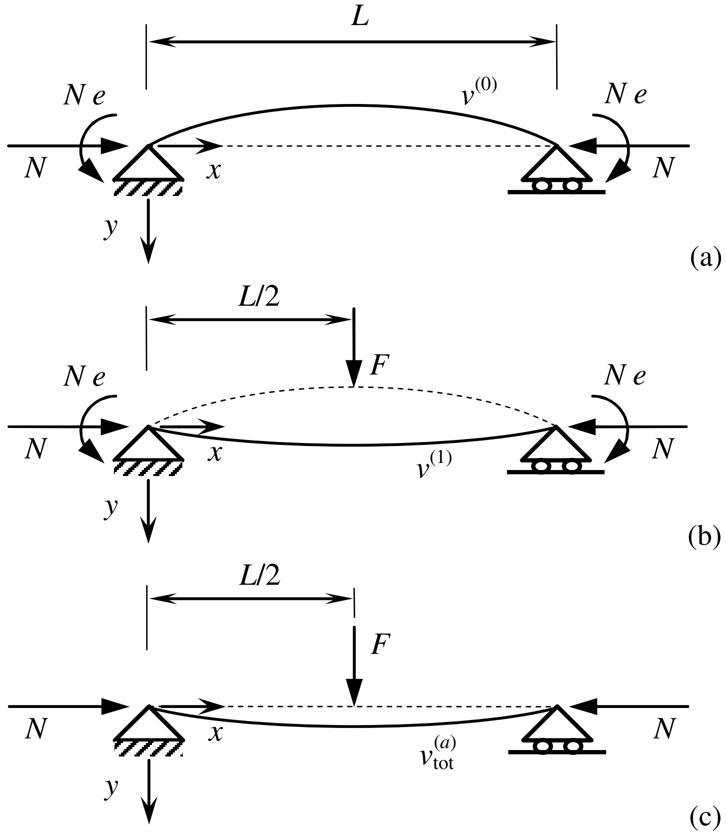

Fig. 1. Reference model of the prestressed concrete beam. (a) Deflection curve $v^{(0)}$ after the application of the eccentric prestress force N, (b) deflection curve $v^{(1)}$ after the application of the vertical load F to deflection curve $v^{(0)}$, and (c) deflection curve $v_{\mathrm{tot}}^{(a)}$ after the application of the vertical load F. The dashed lines correspond to the initial deflection curves.

(a) (b) (c) (d)

Fig. 2. (a) Load cell at one beam end. (b) Hydraulic actuator at the midspan of the beam. (c) Reference LVDT sensor at hinge support. (d) Reference LVDT sensor at roller support.

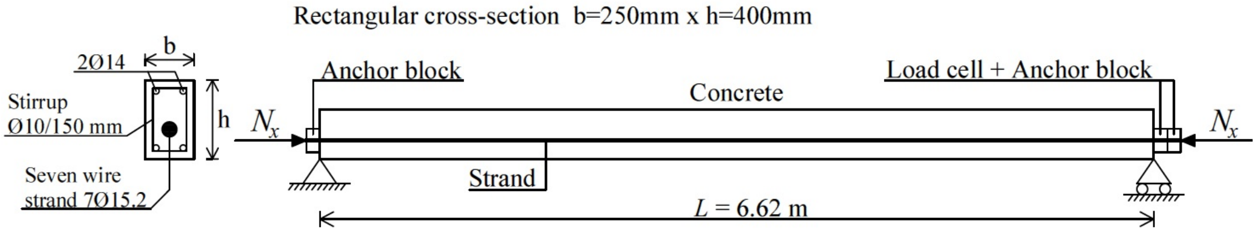

Fig. 3. Scheme of the post–tensioned concrete beam specimen.

(a)

(b)

Fig. 4. (a) Test rig for the NDT method. (b) LVDT sensors along the beam length.

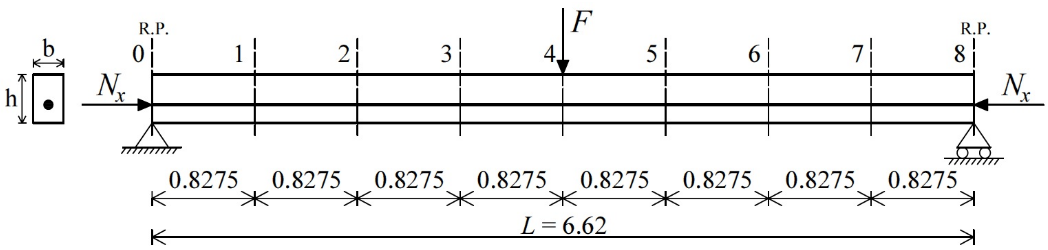

Fig. 5. Test layout with locations of the instrumented sections of the LVDT sensors (values in meters).

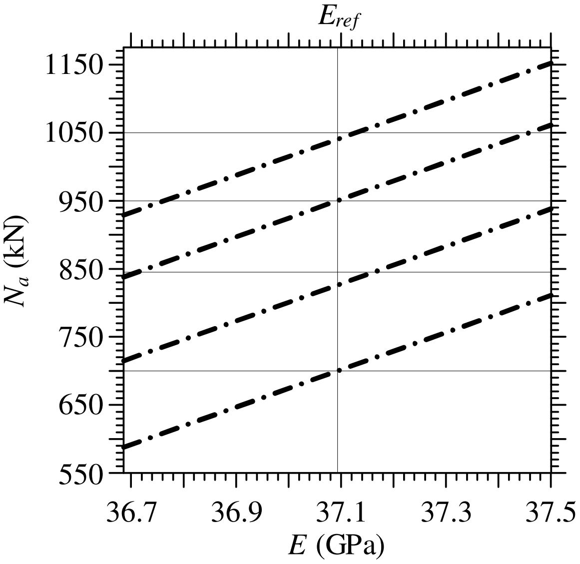

Fig. 6. Numerical three–point bending test. Estimated prestress forces N_a versus elastic modulus E for the four assumed values N_x illustrated in Table 2.

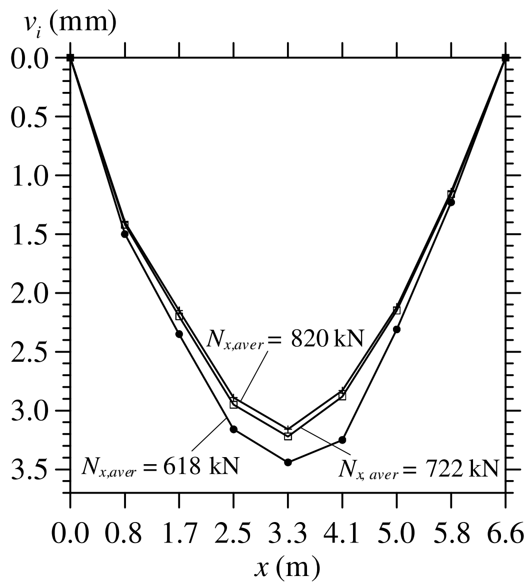

Fig. 7. Experimental three–point bending test. Deflection shape for three prestress forces $N_{x,aver}$ for the F_{aver} = 25.1 kN.

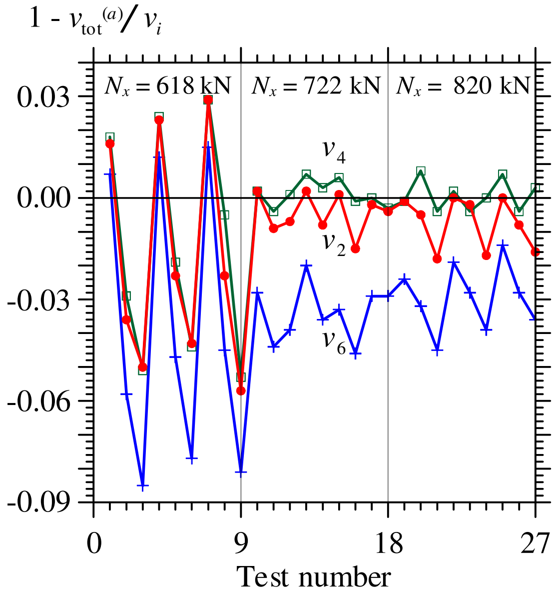

Fig. 8. Error 1 – $v_{tot}^{(a)}/v_i$ versus test number for all test combinations and displacements v_2, v_4, and v_6 depicted in Fig. 5.

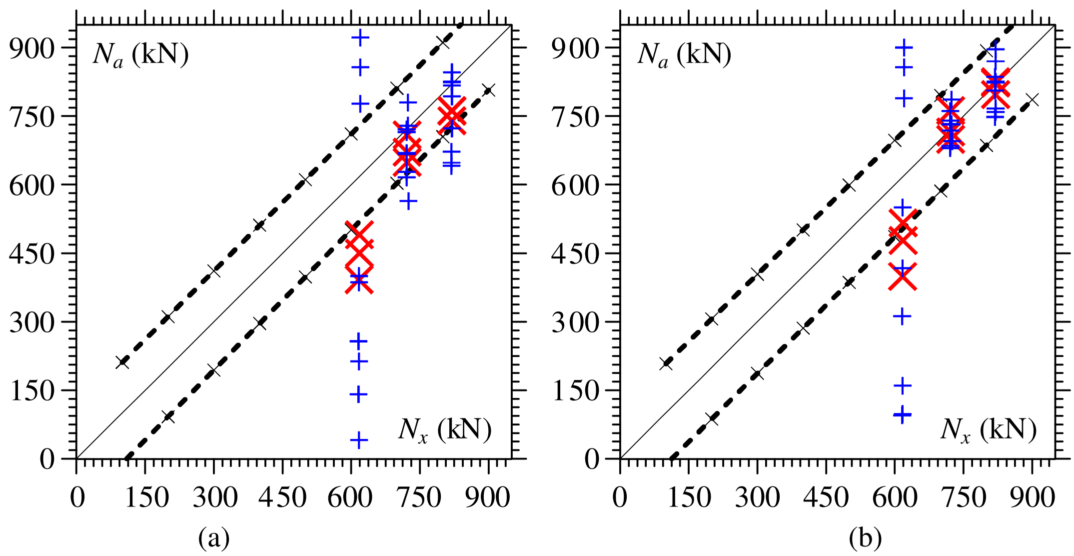

Fig. 9. Prestress force estimates based on (a) Eq. (8a) - Test 1 and (b) Eq. (8b) - Test 2. Symbols + refer to the comparison between estimated N_a and measured values N_x for all 27 test combinations. Symbols ✕ refer to the estimated values $N_{a,aver}$. The dashed lines with symbol ✕ refer to the sensitivity analyses.